OPEN ACCESS
OPUS AUGSBURG

Universität Augsburg
Universitätsbibliothek

Design and mechanical characterisation of a layer wise build AFP insert in comparison to a conventional solution

Alexander Herwig, Peter Horst, Carsten Schmidt, Florentin Pottmeyer, Kay A. Weidenmann

Angaben zur Veröffentlichung / Publication details:

Herwig, Alexander, Peter Horst, Carsten Schmidt, Florentin Pottmeyer, and Kay A. Weidenmann. 2018. "Design and mechanical characterisation of a layer wise build AFP insert in comparison to a conventional solution." *Production Engineering* 12 (2): 121–30. https://doi.org/10.1007/s11740-018-0815-2.

Nutzungsbedingungen / Terms of use:

licgercopyright

Dieses Dokument wird unter folgenden Bedingungen zur Verfügung gestellt: / This document is made available under these conditions:
Deutsches Urheberrecht
Weitere Informationen finden Sie unter: / For more information see:
https://www.uni-augsburg.de/de/organisation/bibliothek/publizieren-zitieren-archivieren/publiz/

Design and mechanical characterisation of a layer wise build AFP insert in comparison to a conventional solution

Alexander Herwig[1] · Peter Horst[1] · Carsten Schmidt[2] · Florentin Pottmeyer[3] · Kay André Weidenmann[3]

Abstract
Joining methods that present a detachable connection of thin walled fiber reinforced plastic (FRP) structures greatly increase the proliferation of lightweight FRP-parts. This paper describes the design of a new layer wise build insert solution named multilayer insert (MLI) in a comparative study in terms of mechanical performance. The MLI is designed to be easily integrable into existing automated fiber placement processes. The mechanical characteristics and damage behavior of the MLI is compared with a commercially available insert serving as reference. Comparable results are obtained by testing the specimen in the same test setup. Both, the results of the MLI and the reference specimen show that a geometrical optimization is able to change the failure modes of the connection thereby keeping the surrounding FRP intact while improving the mechanical performance of the entire component.

Keywords Polymer-matrix composites (PMCs) · Mechanical properties · Joints/joining · Fiber-metal laminate · Embedded load introduction element

1 Introduction

Joining of fiber reinforced plastic (FRP) structures can be achieved by common joining technologies like form closure and adhesive bonding. Friction based joints are problematic since the required normal tension cannot be maintained over longer periods due to creep phenomena within the FRP [1]. While detachable connections are in most cases bolted, high performance joints often use combinations of connection technologies and take the orthotropic topology and mechanical properties of the FRP into account. Potential weaknesses preventing bolted connections in FRP, like its low bearing strength [2], is commercially mitigated by inserting a metallic sleeve, which leads to an even load distribution in the interface layer and increases the available connection surface. Other commercial available joining solutions like bigHead® inserts [3] place a metallic plate within the fiber layers prior the curing process, which is fixated by form closure and adhesive bonding to the matrix material. Connection elements like screws or nuts are used to connect to the inserted plate. Prior investigations developed geometrical guidelines for the plate and have shown that the integration of connector elements into the laminate lead to better results than surface mounted connectors [3–6]. Lightweight structures are typically thin walled, therefore the possible amount of additional material without a noticeable thickening of the structure is limited. An improvement using existing joining methods can therefore mainly be achieved by increasing the acquired form closure, bonding surface or interfacial strength, while keeping the material volume constant.

2 Multilayer insert (MLI)

A common production process for FRP that yields exceptional performance is the automated fiber placement (AFP) process using pre-impregnated (prepreg) fiber tows. The cost and additional effort of the integration into an existing

✉ Alexander Herwig
al.herwig@tu-braunschweig.de

[1] Institute of Aircraft Design and Lightweight Structures, Braunschweig University of Technology, Ottenbecker Damm 12, 21684 Stade, Germany

[2] Institute of Production Engineering and Machine Tools, Leibniz Universität Hannover, Ottenbecker Damm 12, 21684 Stade, Germany

[3] Institute for Applied Materials IAM-WK, Karlsruhe Institute of Technology (KIT), Kaiserstr. 12, 76131 Karlsruhe, Germany

manufacturing process is another important criterion in the manufacturing and adaption of a joint connection within the FRP industry. Therefore, the proposed solution named multilayer insert (MLI, see Fig. 1) is designed to be integrable into existing AFP processes. The metallic insert is generated by locally replacing the prepreg tows with metal sheets (coated with 3M AF 163-2 adhesive [7]) of equal thickness. The stacked sheets form a pure metal area, which can be used as attachment point, surrounded by a hybrid laminate forming the connection to the surrounding laminate (Fig. 1).

The necessary steps within an AFP process are shown in Fig. 2. The prepreg tows are cut to generate a gap that equals the shape of the inserted metal sheet. The gap is then measured by a line scanner, which allows a precise monitoring of the cutting process and placement of the metal sheet. While creating and measuring the gap in the next layer (above), the correct placement and connection to the previous layer (underneath) is checked thermographically [8]. The advantage of this fully automated process is a very low impact on the productivity, a reduction of waste, a very high reproducibility and even more importantly a verified contact and precise positioning of the metal sheets within the prepreg stacking.

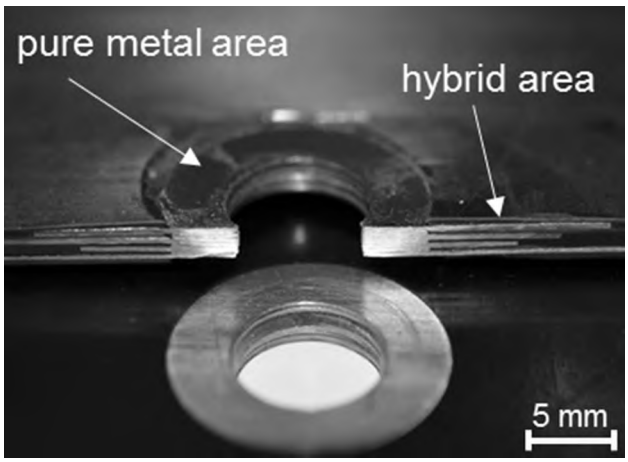

Fig. 1 Close up of the cross section of a MLI with mid hole [8]

There is already a multitude of publications investigating adhesive joints by numerical and analytical means resulting in several recommendations and guidelines for the single and double lap joints. The usage of multiple adhesives or filets to reduce the tension peaks at the free edges is presented in Refs. [10–12]. Numerical investigations regarding more complex joints with asymmetrical [13] or (laminated) composite adherends [14] can be found in more recent investigations. In Ref. [15] the hole bearing capabilities could be improved by alternating between layers of CFRP and titan foils thus forming a hybrid laminate. In most cases the shape of the adherends as well as the shape of the adhesive surfaces are not considered or assumed to be rectangular, thus neglecting effects caused by a complex shape. Within this paper the scope regarding the MLI design will be limited to a geometrically deduction of the available adhesive surface in combination with an estimation of an advantageous bonding length derived from findings in common lap joints.

While the shape of the metal sheets within the placement process can be chosen freely, a first finite-element (FE) assessment of differently shaped metal sheets (ellipses, squares and circles) has shown that the maximal stresses in the surrounding stress field can be reduced by using elliptical

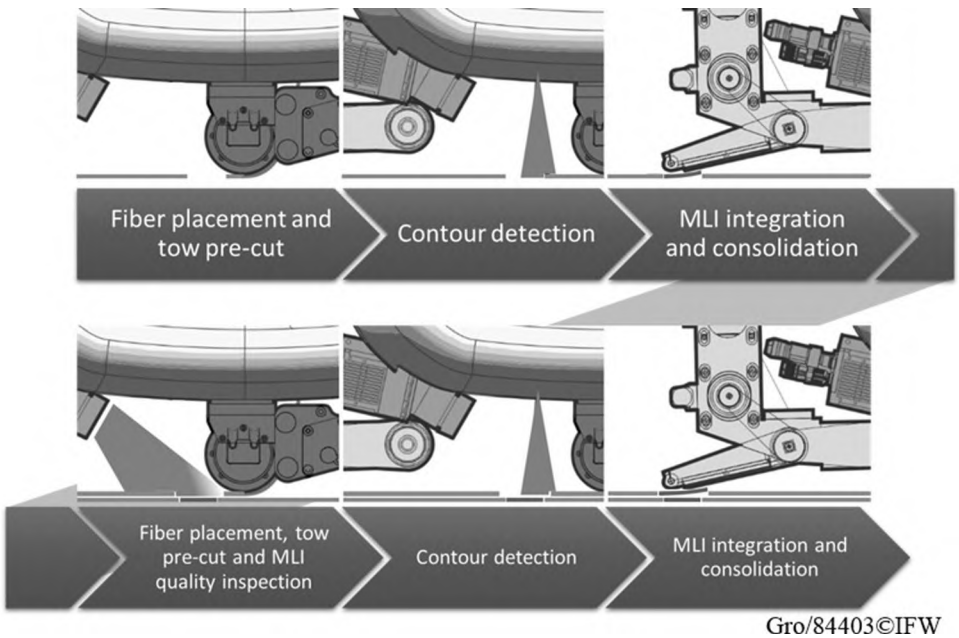

Fig. 2 Building steps of MLI within an AFP process [9]

sheets whose major axis is orientated perpendicular to the fiber orientation. As can be seen in Fig. 3a, the stacking of multiple elliptic metal sheets leads to a centered pure metal area limited in diameter by the minor axis of the smallest ellipse. The free surfaces A_{free} where the metal sheets do not overlap can be used as bonding surface.

2.1 Available bonding surface

As stated before the bonding surface of the load introduction element is an important factor, which greatly affects the achievable performance of the joint. The size of the free surface A_{free} of two overlapping ellipses $E_1\,(a_1,\ b_1,\ \phi_1,\ x_1,\ y_1)$ and $E_2\,(a_2,\ b_2,\ \phi_2,\ x_2,\ y_2)$ is determined by the location of the ellipse center $(x,\ y)$, the semi-major and semi-minor axis a and b as well as the difference in the angle of rotation $\Delta\phi = \phi_2 - \phi_1$, which in this case is predetermined by the stacking of the laminate. The angle θ is used for integration in polar coordinates and is measured between the semi-major axis a and a point on the ellipse. In case of ellipses with a common center the calculation of the overlap area simplifies to the calculation of the difference between the area of the four ellipse sectors and the ellipse surface, as shown in Fig. 3b.

The area calculation of an ellipse sector A_{sec} can be simplified to the calculation of a line integral (Eq. 1) using the Gauss–Green formula [16]. The area depends on the semi-axes a and b as well as the sector angles θ_i and θ_j which are measured from the semi-major axis a to point P_i and P_j.

$$A_{sec}(\theta_i,\ \theta_j,\ a,\ b) = \frac{a \cdot b}{2} \int_{\theta_i}^{\theta_j} dt = \frac{(\theta_j - \theta_i) \cdot a \cdot b}{2} \tag{1}$$

$$A_{sec,E_1} = \int_{\theta(P_2)}^{\theta(P_3)} E_1(a_1,\ b_1) = \frac{(\theta(P_3) - \theta(P_2)) \cdot a_1 \cdot b_1}{2} \tag{2}$$

$$A_{sec,E_2} = \int_{\theta(P_1)}^{\theta(P_2)} E_2(a_2,\ b_2) = \frac{(\theta(P_2) - \theta(P_1)) \cdot a_2 \cdot b_2}{2}. \tag{3}$$

By calculating the difference between the ellipse surface and the overlap area $A_{overlap}$, the available free area A_{free} can be determined.

$$A_{overlap} = 2 \cdot A_{sec,\,E_1} + 2 \cdot A_{sec,\,E_2}. \tag{4}$$

Since the surface areas on top and bottom are the same, the available surface A_b for adhesive bonding is two times the free surface A_{free}.

$$A_b = 2 \cdot A_{free} = 2 \cdot (A_{ellipse} - A_{overlap}). \tag{5}$$

Figure 4a shows the influence of the ratio between the semi-axis (ellipticity) $c = \frac{a}{b}$ on the free surface area for common angular differences in a stacking of identical ellipses. The maximal available surface area for an angular difference of $\Delta\phi = 90°$ can be found at an axis ratio of $c = 0.47$ and at a slightly decreased ratio for the angle differences of 45° and 60°.

An investigated approach for increasing the free surface area is to change the stacking to a double-layer sequence, which consists of layer pairs containing the same angle (Fig. 3c). This change allows for the replacement of every second layer by a small circular spacer. This changes the available bonding surface to the difference in surface area of the ellipse and spacer (Eq. 6).

$$A_{b,\,dl} = 2 \cdot (A_{ellipse} - A_{spacer}). \tag{6}$$

For spacers with a smaller or equal diameter than the semi-minor axis b of the ellipses there is no influence of the angular difference $\Delta\phi$ on the bonding surface. Therefore, the only remaining incentive to change the shape of the spacer or metal sheets within each layer is the spreading of the resulting tension peak in the transition from FRP to metal over a wider area. The resulting surface for a spacer radius that equals the minimal semi-axis in

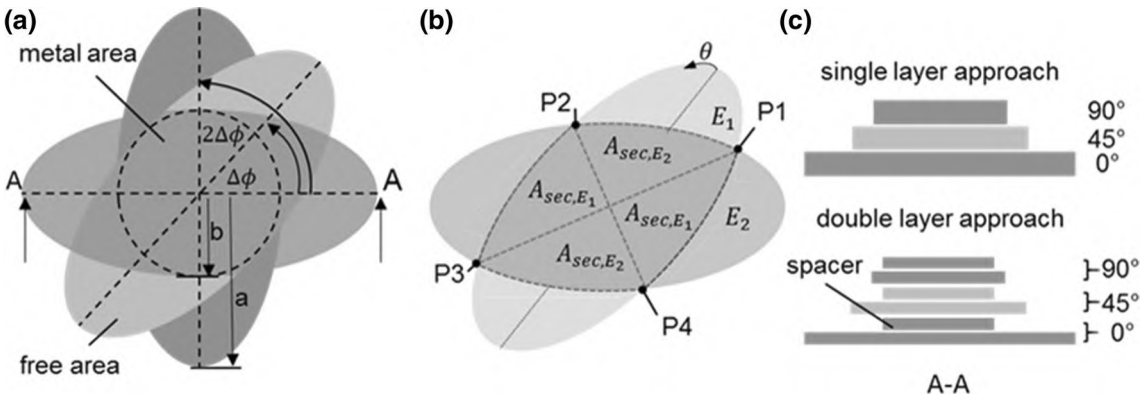

Fig. 3 **a** Available bonding surface of two identical but rotated ellipses and common center. **b** Area segments used for calculation of available bonding area. **c** Difference in stacking for single and double layer approach

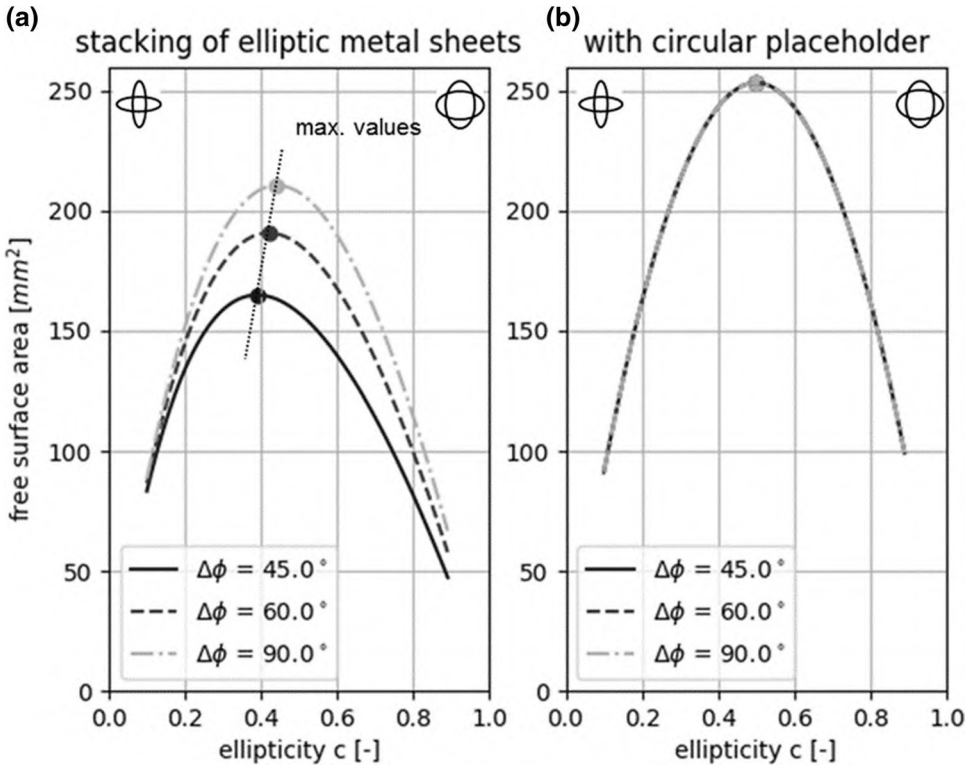

Fig. 4 **a** Free surface area of the enclosed ellipse in a stack of three ellipses (Eq. 5) **b** with placeholder (Eq. 6). The ellipses have the same surface area, a constant angle of rotation $\Delta\phi$ and a common center. The length of the semi-major axis is set to 12.7 mm, while the semi-minor axis is computed accordingly

Table 1 Comparison of the adhesive surface of a MLI metal sheet ($a = r_{circle} = 12.7$ mm, $b = r_{spacer} = 6.35$ mm) in single-layer (without spacer) and double-layer (with spacer) configuration and an eccentricity of c = 0.5

	Adhesive surface (mm^2)
Elliptical	
Single-layer	207
Double-layer	253
Circular	
Single-layer	0
Double-layer	760

the ellipse stacking (as depicted in Fig. 3a) is shown in Fig. 4b with respect to the ellipticity.

The adhesive surface of MLI metal sheets with an ellipticity $c = 0.5$ as used in the experiments in single- and double-layer configuration is given in Table 1.

2.2 Effective bonding length

In a first simple analysis, the load transfer between the MLI layers and the surrounding laminate is simplified to a double shear lap connection of two elastic joint partners, as depicted in Fig. 5. According to this simplification a MLI would be build up by stacking of double shear lap connections. To account for stacking effects only one-half of the top and bottom layer thickness is used in the model. A first analytical description assuming tension in the adherents and shear occurring in the adhesive only can be found in Ref. [10]. A modified model by Tsai et al. [11] also allows for shear in the adherends, which improves the prediction of the maximum values. A detailed description of the presented estimation of an advantageous lap length can be found in Ref. [4] neglecting effects resulting from adherend shear.

In the transition area between FRP and metal, the normal forces within the enclosed layer are transferred via shear into the top and bottom layer. The consideration of elastic joining partners leads to a hyperbolical stress distribution.

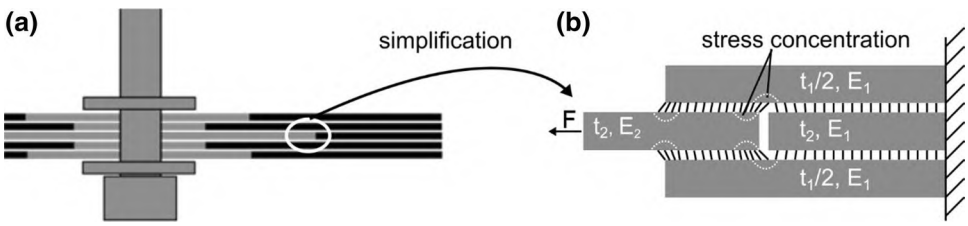

Fig. 5 Schematic of the double shear lap connection **b** used as simplified model of a metal run, **a** out with expected locations of stress concentration

The sizing stress peak $\tau_{adh,\,max}$ can be found at the position of the metal run out according to Eq. 9, with the length of the adhesive connection l_{adh}, τ_{AVG} as the mean shear stress, ψ describing the ratio of the E-Moduli E_i of the adherends and layer thicknesses t_i of the adherends as well as ρ describing the adhesive connection under normal forces. An investigation of the influence of local delamination in the transition area can be found in Ref. [17].

$$\psi = \frac{E_1 \cdot t_1}{E_2 \cdot t_2} \tag{7}$$

$$\rho^2 = (1+\psi)\frac{l_{adh}^2 \cdot G_{adh}}{E_1} \tag{8}$$

$$\frac{\tau_{adh,\,max}}{\tau_{adh,\,AVG}} = \frac{\rho}{2}\left[\coth\left(\frac{\rho}{2}\right) + \frac{1-\psi}{1+\psi}\tanh\left(\frac{\rho}{2}\right)\right]. \tag{9}$$

For $\rho \geq 5$ the stress peak is independent of the hyperbolic parts which evaluate to $\coth\left(\frac{5}{2}\right) \approx \tanh\left(\frac{5}{2}\right) = 1$. The corresponding minimum adhesive length $l_{adh,\,min}$ results to

$$l_{adh,\,min} = 5/\sqrt{\frac{G_{adh}(1+\psi)}{E_1 \cdot t_1 \cdot t_{adh}}}. \tag{10}$$

The material parameter combination within the MLI: $E_2 = E_{steel} = 210$ GPa, $t_2 = t_{steel} = 0.1$ mm, $E_1 = E_{CFRP,\ 0°} = 136$ GPa, $t_1 = t_{CFRP} = 0.1$ mm, $G_{adhesive} = 413$ MPa (taken from product datasheets [7, 18]) and $t_{adh} = 0.07$ mm (microscopically measured) result in an minimum length of the adhesive connection of

$$l_{adh,\,min} = 7.09 \text{ mm}.$$

Above this length, the occurring stress is independent of the bonding length and can only be reduced by a widening of the adhesive area.

3 Insert geometries for mechanical testing

Two joining elements were chosen as mechanical reference for the AFP specimens: (1) the bigHead® (B38H1) as a commercially available insert solution with a circular ground plate diameter of 38 mm and a thickness of 1.2 mm. (2) The self-manufactured D30H1 consisting of bushing welded to a circular ground plate. In addition to that, the clamping of both used CFRP materials (Cycom 977-2 prepreg and NLT00) without an insert was also tested. The NLT00 reference was clamped with two washers d = 30 mm according to the D30H1 diameter, while the Cycom 977-2 prepreg specimen used washers with a diameter of 19 mm. The clamping for the insert-less specimens was done in the same way as shown in Fig. 6b for the MLI specimen. Figures 6a and 7b show the undamaged specimen before testing. For the insert solutions, the inserted ground plate or metal sheets are considered as additional weight. Table 2 gives an overview of the geometrical dimensions and additional weight of each configuration.

The test specimen had to be adjusted to the specific RTM and AFP processes. The AFP specimen comprises of 16 plys Cycom 977-2-35-12KHTS-134 prepreg system with Tenax HTS40 F12 12K 800 tex fibers [18]. The measured specimen have a square shape of 140 × 140 mm^2 and a thickness of 1.6 mm after curing results in a ply thickness of 0.1 mm with a fiber volume fraction of approximately 55%. The MLI semi-axis were chosen to ease manufacturing. The semi-major axis is equivalent to 12.7 mm (the width of two prepreg tows), while the semi-minor axis equals 6.35 mm which corresponds to the width of one prepreg tow (Fig. 6a). Each metal sheet of the circular MLI, which will be referred to as MLI_C, has an adhesive surface of $A_{adh} = 760$ mm^2, while the metal sheets forming the elliptical MLI_E have an adhesive surface of $A_E = 253$ mm^2 (see Table 1). For both MLI the metal sheets are stacked alternating with small circular spacers with a radius equaling the size of the semi-minor axis.

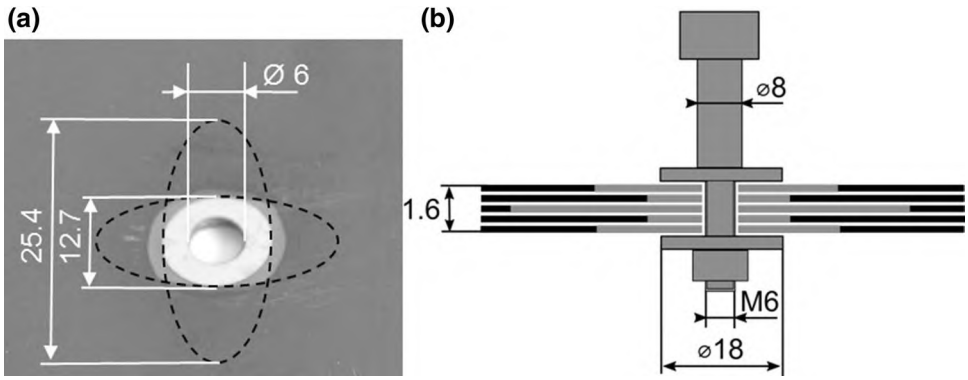

Fig. 6 **a** Undamaged MLI with center hole. **b** Schematic sketch of the fastening element with dimensions used in the experiments (not to scale)

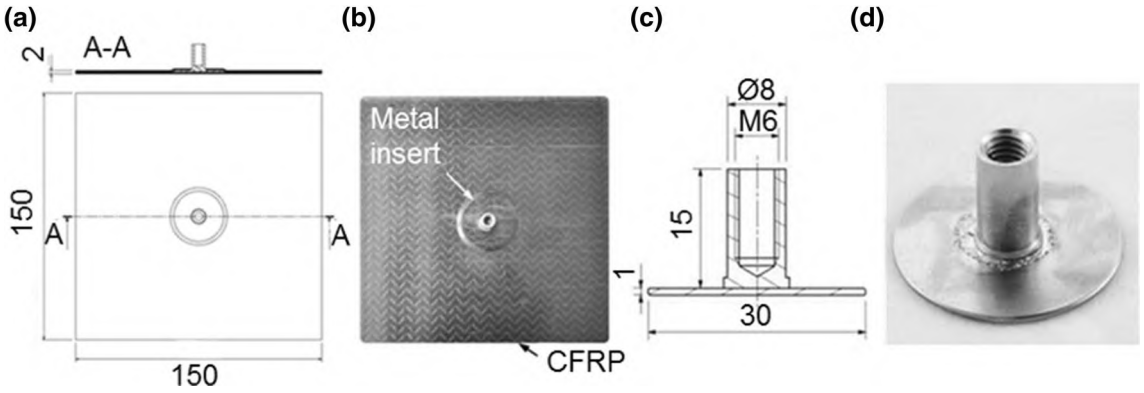

Fig. 7 **a, b** Dimensions and representative picture of the D30H1 specimen. **c, d** Dimensions and representative picture of the D30H1 insert (after Langlais [3])

Table 2 Insert geometries and properties

Insert	Diameter (mm)	Additional weight (g)	Sheet/plate thickness (mm)	Specimen thickness (mm)
B38H1	38	9	1.2	1.6
MLI_C	25.4	4.3	16×0.1	1.6
MLI_E	25.4/12.7	2.6	16×0.1	1.6
D30H1	30	5.6	1	1
Cytec 977-2	18	–	–	1.6
NLT00	30	–	–	2

The inserted ground plate and metal sheets are considered as additional weight for the inserts

Each metal sheet has a thickness of 0.1 mm. The equal thickness of the sheets and the FRP plies minimize changes in the laminate thickness and therefore fiber ondulation in thickness direction. The dimensions of undamaged MLI with center hole as well as the dimensions of the fastening elements can be seen in Fig. 6.

The RTM specimens comprise of eight plies of a biaxial non-woven carbon fiber fabric (Hexcel NLT00 series, 0°/90°, 200 g/m^2) and an epoxy resin by Sika® (Biresin® CR170/CH150-3). The cured specimens have a square shape of 150×150 mm^2 and a measured thickness of 2 mm resulting a in a ply thickness of 0.25 mm and a fiber volume fraction of approximately 44% (Fig. 7). A detailed description of the manufacturing process of the RMT specimen, which is hereinafter referred to as D30H1 describing the diameter and height of the ground plate, can be found in Ref. [3].

4 Experimental setup and specimen preparation

The mechanical characterization is performed by tensile tests using 0°/90° cross ply laminates with an insert placed in the symmetrical plane (Fig. 8). The tensile tests consider pull-out perpendicular to the laminate plane and a typical load case for thin walled structures: in-plane-shear. The tests are carried out on a universal material testing machine (Zwick, F_{max} = 200 kN) at room temperature with a crosshead velocity of 1.5 mm/min. The position of the crosshead is used for the displacement measurement. The specimens are clamped in a mounting frame with a square opening of 80×80 mm^2. A screw fixed with a torque of 8 N m is used to transmit the force into the inserts. As mentioned above, the MLI specimens use additional washers with a diameter of 18 mm to protect the top and bottom layers and prevent damages during fastening. Both the RTM and the B38H1 insert are fastened against the surface of the adapter with a diameter of 24 mm as shown in Fig. 8.

5 Results and discussion

5.1 In-plane-shear test

Figure 9a shows exemplary results of the in-plane-shear tests. The load is introduced by shear into the top and bottom layer of the specimen. Derived from the course of the force displacement curve it can be assumed that after the initial clamp friction is reached at approximately 3 kN, the washers start to slide and the screw is pulled against the CFRP and in case of the MLI against the steel layers. The gradual deterioration of the CFRP specimen due to excessive bearing stress shows itself by force drops. The first drops occur at around 4 kN. The MLI_C and MLI_E specimen endure the highest bearing stresses and fail on

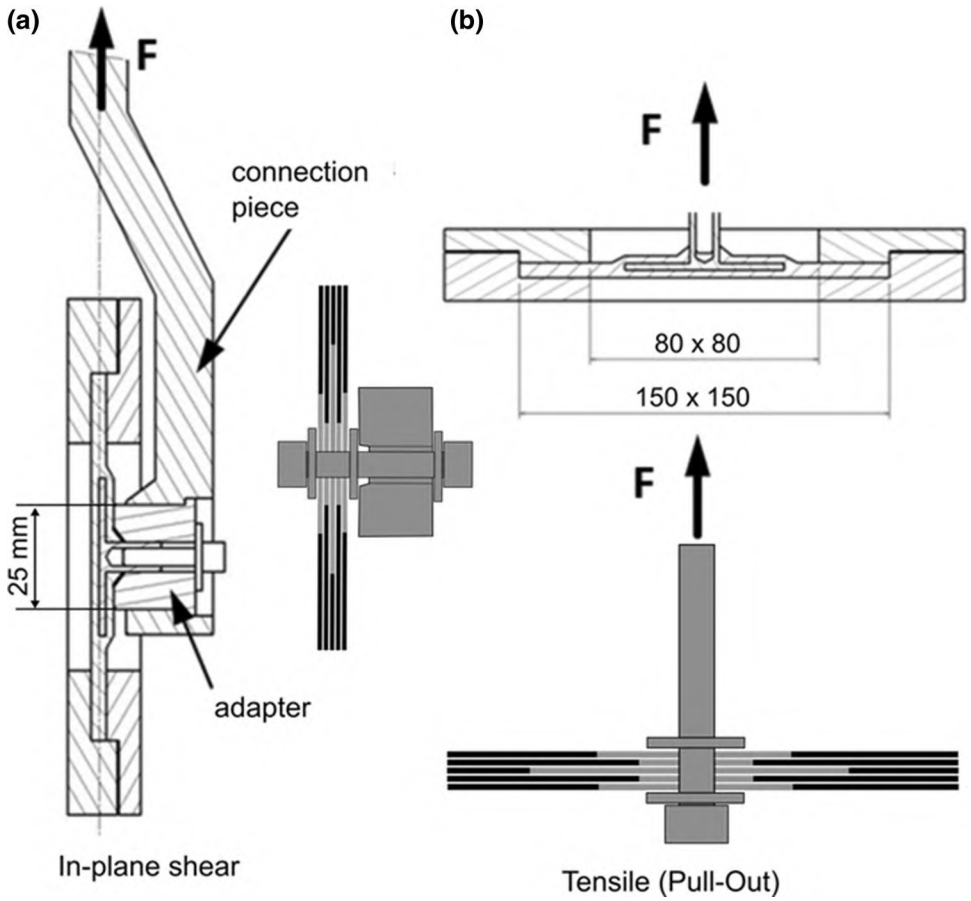

Fig. 8 Devices for the testing of the **a** tensile and **b** shear force cases [3] and the adjusted version with washers on both sides used for the MLI

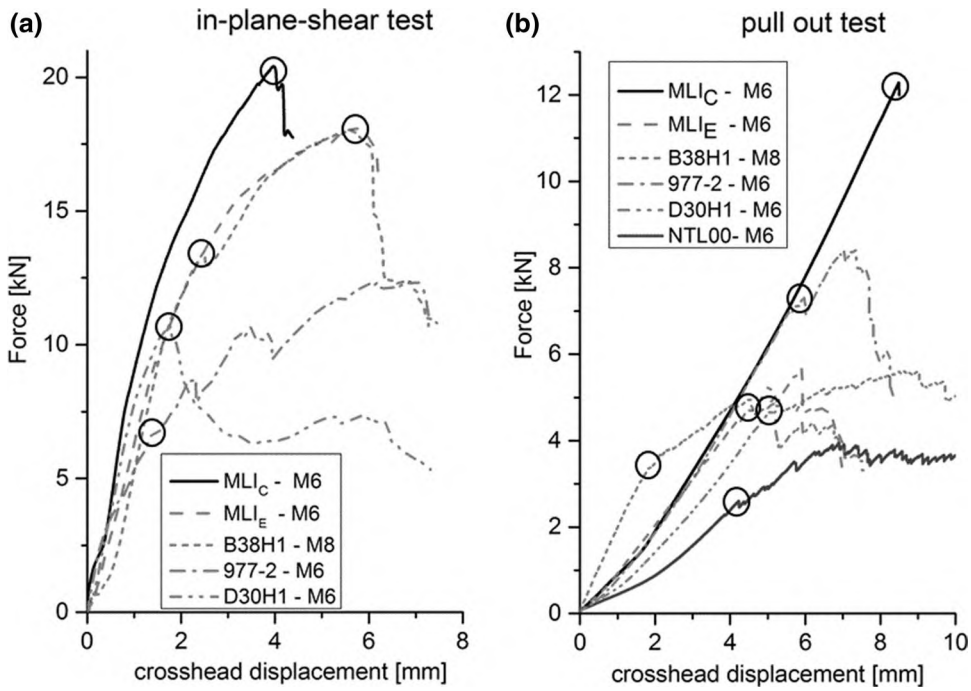

Fig. 9 Representative results of the tested specimen types in the in-plane-shear test (**a**) and the pull out test (**b**). First failures indicated by a discontinuous change in slope were marked

average at 19.8 and 17.4 kN, while the force–displacement curves indicate no prior damages. The mode of failure is changed by the MLI into two consecutive failure phases: Both, the MLI_E and MLI_C exhibit at first a gradual hole bearing failure due excessive bearing stress, followed by a sudden tensile failure of the pure metal area when the displacement reaches the outer radius of the pure metal area (Fig. 10). Up to this point the surrounding CFRP stays intact.

Due to the placement in the symmetric plane, the D30H1 and B38H1 compress half of the laminate layers between the ground plate and the adapter of the testing device. The first slip or delamination occurs on average at a force of 10 and 14.1 kN presumably due to the bigger clamping surface. In Ref. [19] it could be shown that the stud of the D30H1 insert starts deforming plastically at about 7 kN, which causes a change of slope of the force–displacement curve. The D30H1 specimens fail abruptly at approximately 11 kN due to the failure of the co-cured adhesive connection between the boundary plate and CFRP. At this point the insert delaminates and is subsequently pulled through the laminate causing delamination. Small forces can still be transmitted due to form closure. The failure mechanisms of the B38H1 specimen is assumed to occur in a comparable way based on visual inspection during the testing and the course of the force–displacement curve. The final failure is caused by a predetermined breaking point around the threaded bolt.

5.2 Pull out test

The results of the pull out tests are shown in Fig. 9b. The comparatively large diameter and thick ground plates of the B38H1 and D30H1 specimens lead to a steep slope for low displacements, followed by a gradually progressing delamination in a large area around the insert within the mid plane of the laminate. The course of the force–displacement curve of the D30H1 specimen is characterized by the typical progressive failure behavior resulting of crosswise fiber breakage and de-bonding of the insert which can be observed in all specimen [4]. The failed specimens show a strong plastic deformation of the boundary plate, which results in a delamination between the upper and lower plies in the area next to the insert [19]. The first failure of the D30H1 specimen occurs at 4.1 kN, which lies well above the 2.5 kN of the clamped NTL00 specimen.

The MLI_E fails on average at a force of 4.8 kN with a displacement of 4.5 mm. At this point the metal sheets delaminate under a mixed mode loading while being pulled out of laminate, which leads to local damages of the surrounding laminate (see Fig. 11). Due to the separated and equally spaced bonding areas of the ellipses, the failure is stabilized and occurs gradually. The first ply failure of the MLI_C specimens occurs at a force of 9.1 kN in the transition of the hybrid and FRP area due to fiber breaks. The intact hybrid area is then pulled out of the surrounding FRP. The effect is enhanced by the manufacturing

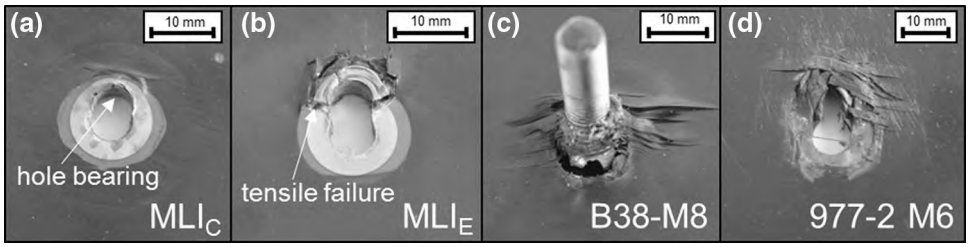

Fig. 10 Failed specimen after the in-plane shear test. The MLI specimen exhibit two consecutive damage states. After the initial hole bearing failure (**a**), the MLI specimen exhibit a tensile failure of the metal area and surrounding fibers (**b**). **c, d** An advancing delamination over a large area in combination with fiber and inter-fiber fractures

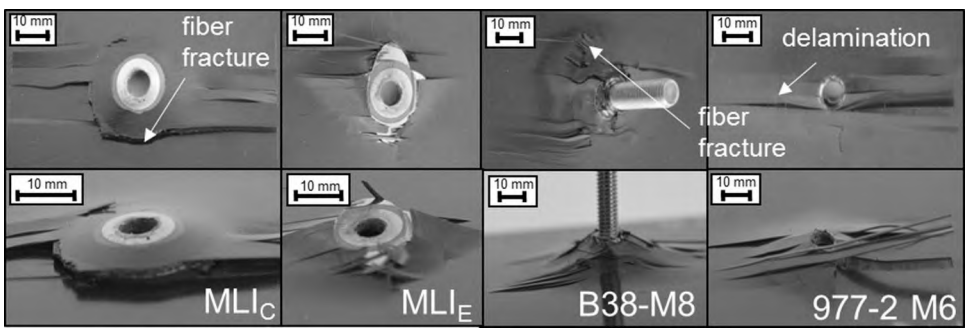

Fig. 11 Failed specimen after the pull out test in top and side view. The detailed description of the D30H1 failure behavior can be found in Ref. [19]

Table 3 Results with standard deviation of the five tested specimen in the pull out and in-plane shear test

Insert	F_{shear} (kN)	$F_{pullOut}$ (kN)	F_{shear}/add. weight (kN/g)	$F_{pullOut}$/ add. weight (kN/g)
B38H1	14.0 ± 1.7	3.6 ± 0.3	1.6 ± 0.19	0.4 ± 0.03
MLI_C	19.8 ± 1.1	9.1 ± 2.3	4.6 ± 0.26	2.1 ± 0.53
MLI_E	17.4 ± 0.7	4.8 ± 0.2	6.7 ± 0.27	1.8 ± 0.07
D30H1	10 ± 1.5	4.1 ± 0.5	1.8 ± 0.26	0.7 ± 0.09
Cytec 977-2	3.9 ± 0.8	5.8 ± 0.7	0.7 ± 0.15	1.0 ± 0.13
NLT00	–	2.5	0.0	0.2

simplification of using sheets and spacers with constant diameters. The variation of the sheet diameters in each layer is expected to distribute the stress over a larger area, thus leading to an improved result. An investigation of the stress concentration in the metal run outs can be found in.

The results of all specimen types in the pull out test strongly depend on the exact vertical position of the load introduction element. This is especially a problem for the clamped CFRP and circular MLI_C specimen since the fixation of the two washers often leads to a tilted load introduction, which induces a bending moment and an accelerated failure due to fiber breaks at the outer edges of the insert. The petal-like geometry formed by the metal sheets of the MLI_E ellipses is less sensitive to a tilted load introduction, which results in a smaller deviation in the results. The mean values and standard deviations of both tests are show in Table 3.

The CFRP clamped between two washers leads to high reaction forces in the tensile test, but has several weaknesses. The first weakness is first ply failure indicated by audible cracking sounds presumably due to delamination or fiber breaks. These failure mechanisms are initiated by the uneven load introduction due to the used washers. After first ply failure, the laminate is damaged by the locating pin, which is pulled through the laminate comparable to the damage of MLI_C shown in Fig. 11. The second problem is the loss of clamping force over an extended time period due to relaxation of the laminate, which is not addressed in this investigation due to the short clamping time.

The bigHead® yields high maximal force values resulting from its huge diameter. The slope is comparable to the other graphs at low displacements, but fails at a displacement of approximately 2 mm due to delamination which leads to a decrease of slope. The following measured forces are achieved by form closure. Any additional displacement leads to delamination and damages to the surrounding laminate.

6 Summary

A comparative study regarding the performance of detachable connection elements for load introduction into CFRP structures has been carried out. The load bearing capacities of embedded metal elements, so-called inserts, were compared to those of usual bolted joints and clamped CFRP.

The commercially available metallic inserts utilize the advantage of the thick metal plate expressed by the steep slope in the force displacement curves; resulting in a stiff joint for low displacements with the disadvantages of an extended delamination area in the insert plane for moderate displacements. This leads to a bigger damaged area which has to be repaired.

Despite the geometrical differences like e.g. the different diameters or thicknesses of the ground plate an improving trend in the maximal forces and slope of the force displacement curves can be observed. This indicates an improvement in the damage evolution during failure, an increased the stiffness of the joint connection and an increase of the failure load by using the proposed insert. While the absolute results of the circular metal sheets appear to be better than the results of the elliptic sheets, one also has to take the amount of inserted metal into account, which is reduced by 40% for the elliptic variant compared to the MLI_C. When using circular and elliptical metal sheets of the same weight, the circular diameter would be significantly reduced and thus be expected to lead to inferior results. The failure process of the MLI is absent of damages like delamination prior to the final failure. The reduced damaged area allows at least in the shear load case for an easier repair. A possible MLI design goal to fully utilize the MLI potential would be a simultaneously occurring hole bearing and delamination failure at the same load level. A limitation of the introduced load and prevention of (laminate) damages could then be easily realized by designed failure points in the connection element to the MLI.

Acknowledgements This paper is based on investigations of the subproject 3—"Fundamental research of intrinsically produced FRP-/metal-composites—from embedded insert to load bearing hybrid structure" and subproject 1—"Multilayer Inserts-intrinsic hybrid compounds for load introduction into thin walled high-performance CFRP structures" of the priority program 1712 "Intrinsic hybrid composites for lightweight load-bearings", which is kindly supported by the German Research Foundation (DFG). The authors kindly acknowledge the Institute for Production Science (wbk) of KIT for the manufacturing of the D30H1 specimen within the cooperation in the abovementioned subproject.

References

1. Scott DW, Lai JS, Zureick A-H (1995) Creep behavior of fiber-reinforced polymeric composites: a review of the technical literature. J Reinf Plast Compos 14(6):588–617. https://doi.org/10.1177/073168449501400603
2. Camanho P, Hallett SR (2011) Composite joints and connections: principles, modelling and testing. Elsevier, Amsterdam
3. Langlais C (2015) Poster presentation at Cranfield University. Preparation and attachment technique for steel fasterners for carbon fibre composite automotive panels. https://www.bighead.co.uk/wp-content/uploads/2015/10/Charles-Langlais-poster.pdf. Accessed 16 Feb 2018
4. Schürmann H (2007) Konstruieren mit Faser-Kunststoff-Verbunden. Springer, Berlin
5. Hoa SV, Di Maria A, Feldman D (1987) Inserts for Fastening Sheet Molding Compounds. In: Marshall IH (ed) Composite structures 4: analysis and design studies, vol 1. Springer, Dordrecht, pp 86–99
6. Ferret B, Anduze M, Nardari C (1998) Metal inserts in structural composite materials manufactured by RTM. Compos Part A Appl Sci Manuf 29(5–6):693–700. https://doi.org/10.1016/S1359-835X(97)00107-3
7. 3M (2009) Scotch-Weld™ structural adhesive film—technical datasheet: AF 163–2
8. Schmidt C, Denkena B, Gross L et al (2017) Concept for automated production of CFRP-metal hybrid compounds integrated in an automated fiber placement process. Procedia 5CIRP6 62:56–61. https://doi.org/10.1016/j.procir.2016.06.046
9. Grützner R, Stefaniak D, Koch SF et al (2016) Intrinsic hybrid composites for lightweight structures: new process chain approaches. WGP Congress 2016, vol 1140. Trans Tech Publications, pp 239–246
10. Volkersen O (1953) Die Schubkraftverteilung in Leim-, Niet-und Bolzenverbindungen. Energie Technik 5(3):5, 7
11. Tsai MY, Oplinger DW, Morton J (1998) Improved theoretical solutions for adhesive lap joints. Int J Solids Struct 35(12):1163–1185. https://doi.org/10.1016/S0020-7683(97)00097-8
12. da Silva LFM, das Neves PJC, Adams RD et al (2009) Analytical models of adhesively bonded joints—Part I: literature survey. Int J Adhes Adhes 29(3):319–330. https://doi.org/10.1016/j.ijadhadh.2008.06.005
13. Ozel A, Yazici B, Akpinar S et al (2014) A study on the strength of adhesively bonded joints with different adherends. Compos Part B Eng 62(Suppl C):167–174. https://doi.org/10.1016/j.compositesb.2014.03.001
14. Tsai MY, Morton J (2010) An investigation into the stresses in double-lap adhesive joints with laminated composite adherends. Int J Solids Struct 47(24):3317–3325. https://doi.org/10.1016/j.ijsolstr.2010.08.011
15. Camanho PP, Fink A, Obst A et al (2009) Hybrid titanium-CFRP laminates for high-performance bolted joints. Compos Part A Appl Sci Manuf 40(12):1826–1837. https://doi.org/10.1016/j.compositesa.2009.02.010
16. Hughes GB, Chraibi M (2012) Calculating ellipse overlap areas. Comput Vis Sci 15(5):291–301
17. Herwig A, Woidt M, Horst P (2016) Comparison of one-, two- and three-dimensional models of a metallic insert in a composite. Key Eng Mater 713:175–178. https://doi.org/10.4028/www.scientific.net/KEM.713.175
18. Cytec Engineering Materials (2012) CYCOM 977-2 epoxy resin system—technical data sheet. https://www.cytec.com/sites/default/files/datasheets/CYCOM_977-2_031912.pdf. Accessed 16 Feb 2018
19. Gebhardt J, Pottmeyer F, Fleischer J et al (2015) Characterization of metal inserts embedded in carbon fiber reinforced plastics. MSF 825–826:506–513. https://doi.org/10.4028/www.scientific.net/MSF.825-826.506